PCCP

^{13}C-^{13}C Spin-Coupling Constants in Crystalline ^{13}C-Labeled Saccharides: Conformational Effects Interrogated by Solid-State ^{13}C NMR Spectroscopy

Journal:	*Physical Chemistry Chemical Physics*
Manuscript ID	CP-ART-06-2019-003228.R1
Article Type:	Paper
Date Submitted by the Author:	24-Sep-2019

Complete List of Authors:	Serianni, Anthony; University of Notre Dame, Department of Chemistry and Biochemistry; Omicron Biochemicals Inc., Zhang, Wenhui; University of Notre Dame, Department of Chemistry and Biochemistry Yoon, Mi-Kyung; University of Notre Dame, Department of Chemistry and Biochemistry Meredith, Reagan; University of Notre Dame, Department of Chemistry and Biochemistry Zajicek, Jaroslav; University of Notre Dame, Department of Chemistry and Biochemistry Oliver, Allen; University of Notre Dame, Department of Chemistry and Biochemistry Hadad, Matthew; University of Notre Dame, Department of Chemistry and Biochemistry Frey, Michael; Jeol USA, Inc. Carmichael, Ian; University of Notre Dame, Radiation Laboratory and Department of Chemistry & Biochemistry

^{13}C-^{13}C Spin-Coupling Constants in Crystalline ^{13}C-Labeled Saccharides: Conformational Effects Interrogated by Solid-State ^{13}C NMR Spectroscopy

Wenhui Zhang,[1] Mi-Kyung Yoon,[1] Reagan J. Meredith,[1] Jaroslav Zajicek,[1] Allen G. Oliver,[1] Matthew Hadad,[1] Michael H. Frey,[3] Ian Carmichael,[2] and Anthony S. Serianni[1]*

[1]Department of Chemistry and Biochemistry, and [2]Radiation Laboratory, University of Notre Dame, Notre Dame, IN 46556-5670; [3]JEOL USA, Inc., 11 Dearborn Rd., Peabody, MA 01960 USA

*Author for correspondence: aseriann@nd.edu

Abstract

Solid-state ^{13}C NMR spectroscopy has been used in conjunction with selectively ^{13}C-labeled mono- and disaccharides to measure ^{13}C-^{13}C spin-couplings (J_{CC}) in crystalline samples. This experimental approach allows direct correlation of J_{CC} values with specific molecular conformations since, in crystalline samples, molecular conformation is essentially static and can be determined by x-ray crystallography. J_{CC} values measured in the solid-state in known molecular conformations can then be compared to corresponding J_{CC} values calculated in the same conformations using density functional theory (DFT). The latter comparisons provide important validation of DFT-calculated *J*-couplings, which is not easily obtained by other approaches and is fundamental to obtaining reliable experiment-based conformational models from redundant *J*-couplings by *MA'AT* analysis. In this study, representative $^1J_{CC}$, $^2J_{CCC}$ and $^3J_{COCC}$ values were studied as either intra-residue couplings in the aldohexopyranosyl rings of monosaccharides or inter-residue (trans-glycoside) couplings in disaccharides. The results demonstrate that (a) accurate J_{CC} values can be measured in crystalline saccharides that have been suitably labeled with ^{13}C, and (b) DFT-calculated J_{CC} values compare favorably with those determined by solid-state ^{13}C NMR when molecular conformation is a constant in both determinations.

Introduction

Spin-spin coupling constants (J-couplings) are valuable NMR parameters in studies of molecular structure. $^{1}J_{CH}$ values depend on the *s*-character of the C–H bond,[1–4] $^{2}J_{HCH}$ values depend on the H–C–H valence bond angle,[5,6] and $^{3}J_{HCCH}$ values depend on the H–C–C–H torsion angle subtended by the coupled hydrogens (Karplus relationship).[7,8] In the β-D-glucopyranosyl ring **1** (Scheme 1), more than sixty J-couplings involving hydrogen and carbon can be measured, and their magnitudes and signs report on a wide range of structural properties, including ring conformation, exocyclic hydroxymethyl group conformation (ω), and exocyclic C–O bond conformation (θ_1 and θ_2).[9] Interactions between the lone-pair orbitals on oxygen and the bonding or antibonding orbitals in structures like **1** exert a major influence on J-couplings, as discussed in recent reviews.[9,10] Because the exocyclic C–O torsional properties of saccharides in solution are not well understood at present, a heavy reliance is placed on theoretical calculations, most notably density functional theory (DFT), to identify and quantify lone-pair effects on molecular structure, and on molecular dynamics (MD) simulations to predict their time-dependent behaviors.[10]

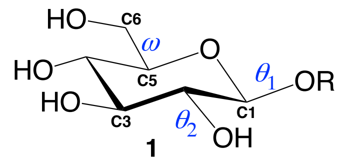

1

Scheme 1. The β-D-glucopyranosyl ring (**1**) illustrating two exocyclic C–O torsion angles, θ_1 (C1–O1) and θ_2 (C2–O2), and an exocyclic C5–C6 torsion angle (ω).

Experimental NMR J-couplings measured in solution are often averaged by molecular motion. For example, rotations of the two exocyclic C–O bonds, θ_1 and θ_2, in **1** affect the value of $^{1}J_{C1,C2}$.[11] Rotation of the C2–O2 bond θ_2 significantly affects the geminal $^{2}J_{C1,C3,}$ whereas the effect of rotating θ_1 is small.[9] Rotation of the C5–C6 bond ω affects $^{3}J_{C1,C6}$ due to the changing disposition of O6 with respect to the C1–O5–C5–C6 coupling pathway.[12,13] In this case, while the C1–O5–C5–C6 torsion angle remains constant at ~180° (imposed by ring conformation), the secondary terminal electronegative substituent effect from O6 depends on ω. In the disaccharide, methyl β-D-galactopyranosyl-(1→4)-β-D-glucopyranoside (**2**) (Scheme 2), rotation of the internal *O*-glycosidic C–O bond *psi* (ψ) changes the C1'–O1'–C4–C5 torsion angle, which in turn affects the trans-glycoside $^{3}J_{C1',C5}$ value. Interrogating these rotational effects can be accomplished in some cases by studying conformationally constrained molecules in solution, or by computational methods.[10,14] Experimental measurements on crystalline saccharides having defined (and fixed) conformations would complement these existing approaches and add a valuable new dimension to assist in structural and conformational interpretations of time-dependent NMR *J*-couplings in solution. This approach eliminates the uncertainties introduced when flexible molecules are constrained covalently to reduce their motions in solution, but which often contain coupling pathways that no longer resemble those in the free (unconstrained) molecules.

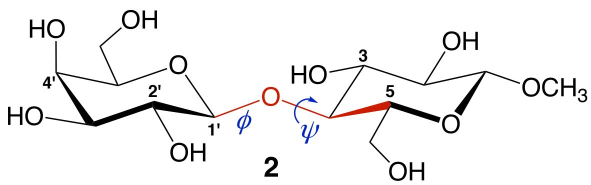

2

Scheme 2. Structure of methyl β-D-galactopyranosyl-(1→4)-β-D-glucopyranoside (βGal-(1→4)-βGlcOCH$_3$) (**2**) showing the internal *O*-glycosidic torsion angles, *phi* (ϕ) and *psi* (ψ), and highlighting the C1'–O1'–C4–C5 coupling pathway (in red) across the linkage.

Solid-state NMR (ssNMR) has been used previously to measure NMR scalar couplings in crystalline or disordered solid samples.[15] Broad lines are usually observed in 1D spectra due to anisotropic interactions, making the extraction of *J*-couplings from the splittings of signals difficult, especially for relatively small long-range *J*-couplings.[16–18] The use of spin-echo magic-angle-spinning (MAS)-based experiments eliminates this problem and allows routine determinations of *J*-couplings in both organic and inorganic solid samples.[19–26] To measure J_{CC} values in organic compounds, the sensitivity of the MAS experiment can be increased by applying a cross-polarisation (CP) pulse sequence.[17,27,28] Recent work by Brown[29] and Thureau[30], using selective spin-echo experiments, has shown that long-range *J*-couplings between two spin-1/2 heavy nuclei can be measured in crystalline solids with high accuracy. These *J*-values are associated with fixed (or highly constrained) conformations of a molecule, thus eliminating the challenges of interpreting them in the presence of motional averaging in solution. In saccharides, this opportunity is particularly germane because, in crystalline solids, their exocyclic C–O torsions are highly constrained by extensive hydrogen bonding in the lattice, thus allowing direct comparisons between experimental *J*-couplings and those calculated in conformationally identical structures by DFT. These comparisons are vital to efforts directed towards validating *J*-couplings calculated by DFT.

With the above validation in mind, three doubly ^{13}C-labeled monosaccharides and two doubly ^{13}C-labeled disaccharides (Scheme 3) were prepared to enable measurements of ^{13}C-^{13}C spin-couplings in crystalline samples: methyl β-D-[1,2-$^{13}C_2$]glucopyranoside (**3**^{1,2}), methyl β-D-[1,3-$^{13}C_2$]glucopyranoside (**3**^{1,3}), methyl β-D-[1,6-$^{13}C_2$]glucopyranoside (**3**^{1,6}), methyl β-D[1-^{13}C]galactopyranosyl-(1→4)-β-D-[5-^{13}C]glucopyranoside (**2**$^{1',5}$), and methyl β-D-galactopyranosyl-(1→4)-α-D-[5-^{13}C]glucopyranoside (**4**$^{1',5}$) (see the definition of superscripts in Scheme 3). These compounds were easily crystallized[31–33] and reliable synthetic methods were available to introduce ^{13}C (~99 atom-%) selectively at the indicated sites. The relative rigidity of the β-D-glucopyranosyl ring ($^4C_1$ conformer) of **3** in solution and in crystalline samples eliminated potential conformational contributions to the measured J_{CC} values, such as rotation of the endocyclic C1–C2 bond that may occur from ring pseudorotation[34], which can affect $^1J_{C1,C2}$,[11] and rotation of the endocyclic C5–

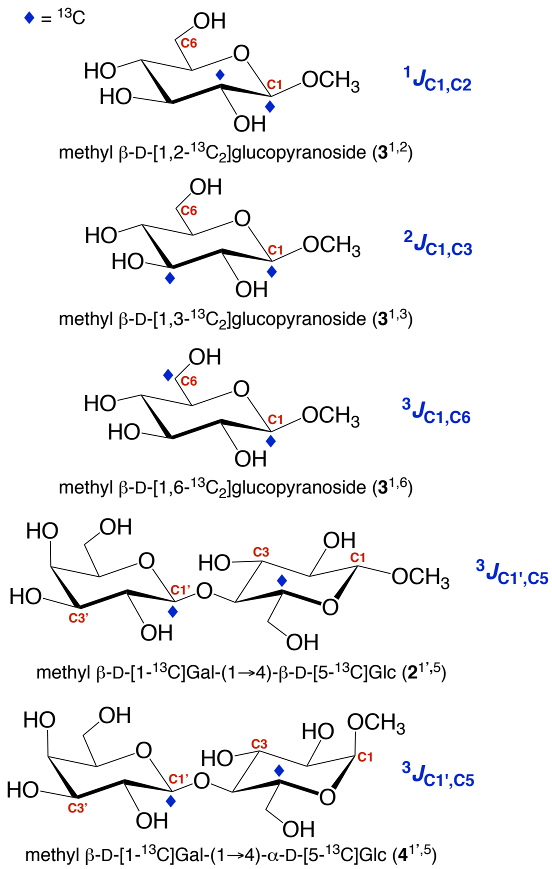

Scheme 3. Chemical structures of the five selectively ^{13}C-labeled mono- and disaccharides used in this study, and the J_{CC} value measured in each compound by solution and solid-state ^{13}C NMR. Superscripts on the compound numbers denote the carbons that were labeled with ^{13}C in each compound.

O5 bond, which can affect $^{3}J_{C1,C6}$.[13,14,35] Similar ring rigidity in both residues of **2** and **4** simplified the analysis of the trans-*O*-glycosidic $^{3}J_{C1',C5}$ value.

Experimental

*A. Synthesis of ^{13}C-Labeled **2–4**.* Compounds $\mathbf{3}^{1,2}$, $\mathbf{3}^{1,3}$ and $\mathbf{3}^{1,6}$ were prepared from D-[1,2-$^{13}C_2$]glucose ($\mathbf{5}^{1,2}$), D-[1,3-$^{13}C_2$]glucose ($\mathbf{5}^{1,3}$) and D-[1,6-$^{13}C_2$]glucose ($\mathbf{5}^{1,6}$), respectively. Compound $\mathbf{5}^{1,2}$ was prepared from D-[1-^{13}C]arabinose and K^{13}CN by cyanohydrin reduction.[36,37] Compound $\mathbf{5}^{1,3}$ was prepared from D-[2-^{13}C]arabinose and K^{13}CN by cyanohydrin reduction;[36,37] D-[2-^{13}C]arabinose was prepared from D-[1-^{13}C]erythrose and unlabeled KCN by cyanohydrin reduction,[36,37] or from D-[1-^{13}C]ribose[36,37] by molybdate-catalyzed C2-epimerization.[37,38] Compound $\mathbf{5}^{1,6}$ was prepared from 1,2-*O*-isopropylidene-α-D-[1-^{13}C]glucofuranose and K^{13}CN.[39] Laboratory procedures to convert $\mathbf{5}^{1,2}$, $\mathbf{5}^{1,3}$ and $\mathbf{5}^{1,6}$ into $\mathbf{3}^{1,2}$, $\mathbf{3}^{1,3}$ and $\mathbf{3}^{1,6}$, respectively, and to prepare disaccharides $\mathbf{2}^{1',5}$ and $\mathbf{4}^{1',5}$ (Scheme S1) are provided in the Supporting Information.

Compounds $\mathbf{3}^{1,2}$, $\mathbf{3}^{1,3}$ and $\mathbf{3}^{1,6}$ were crystallized from a concentrated aqueous solution, and $\mathbf{2}^{1',5}$ and $\mathbf{4}^{1',5}$ were crystallized from anhydrous methanol. The structures and purities of $\mathbf{2}^{1',5}$, $\mathbf{3}^{1,2}$, $\mathbf{3}^{1,3}$, $\mathbf{3}^{1,6}$ and $\mathbf{4}^{1',5}$ were confirmed by high-resolution mass spectrometry (Table S1, Supporting Information) and solution NMR spectroscopy (Figures S1–S5, Supporting Information).

*B. X-Ray Crystallography of ^{13}C-Labeled **2–4**.* An arbitrary sphere of data was collected on colorless crystals of $\mathbf{2}^{1',5}$, $\mathbf{3}^{1,2}$, $\mathbf{3}^{1,3}$, $\mathbf{3}^{1,6}$ and $\mathbf{4}^{1',5}$ using a Bruker APEX-II diffractometer and a combination of ω- and ϕ-scans of 0.5°. The crystallographic structures obtained for each sample were identical to those reported previously.[31–33]

*C. Measurements of ^{13}C-^{13}C Spin-Couplings in ^{13}C-Labeled **2–4** in Aqueous ($^{2}H_2O$) Solution.* High-resolution 1D ^{13}C{^{1}H} NMR spectra were obtained on $\mathbf{2}^{1',5}$, $\mathbf{3}^{1,2}$, $\mathbf{3}^{1,3}$, $\mathbf{3}^{1,6}$ and $\mathbf{4}^{1',5}$ using 5-mm NMR tubes on a Varian DirectDrive 600-MHz FT-NMR spectrometer equipped with a 5-mm ^{1}H-^{19}F/^{15}N-^{31}P AutoX dual broadband probe. Spectra were collected in $^{2}H_2O$ at 22 °C with ~15,000 Hz spectral windows and ~4.5 s recycle times, and were processed to give final digital resolutions of ~0.05 Hz/pt. ^{13}C-^{13}C Spin-couplings were obtained by analysis of the doublet character of the two intense signals arising from the mutually coupled ^{13}C-labeled carbons in each compound (Figures S1–S5, Supporting Information). Since one of the ^{13}C-labeled carbons in each of the five compounds is an anomeric carbon, non-first-order effects on the measurements of the J_{CC} values were negligible.

*D. Measurements of ^{13}C-^{13}C Spin-Couplings in Crystalline ^{13}C-Labeled **2–4**.* Crystalline samples of **2**$^{1',5}$, **3**^{1,2}, **3**^{1,3}, **3**^{1,6} and **4**$^{1',5}$ (~40 mg of each) were mixed with KBr (60:40 *w/w* sample:KBr) to give samples that contained an internal standard for *in situ* magic angle calibration. All NMR measurements were performed on a JEOL ECX-300 solid-state FT-NMR spectrometer operating at a ^{1}H frequency of 300 MHz and equipped with a 3.2-mm magic angle spinning (MAS) probe. The magic angle (54.74°) was carefully adjusted on each sample by monitoring the ^{79}Br signal arising from the internal KBr; spinning sidebands were observed to ~8 ms. The MAS frequency was set to 16 kHz. Prior to making the J_{CC} measurements, cross polarization (CP) MAS ^{13}C NMR spectra were recorded on each sample using a standard CP pulse sequence, a 1.97 μs ^{1}H 90° pulse, and a 1.5 ms contact time.

For the measurement of ^{13}C-^{13}C spin-couplings, the pulse sequences for the reference (S_o) and *J*-modulated (*S*) experiments were programmed into the spectrometer as described by Thureau and coworkers.[30] The reference signals were obtained using a single-band selective 180° Gaussian function, and the *J*-modulated signals were obtained using a double-band selective 180° Gaussian function multiplied by a cosine wave. The signal amplitude was expressed as a function of the total echo interval, τ, where $\tau = 2\tau_{ev} + \tau_p$, τ_{ev} represents the free evolution time, and τ_p represents the duration of the selective 180° pulse. The value of τ_p was held constant at 5 ms, while $2\tau_{ev}$ was systematically increased in 3-ms increments from 0 – 51 ms (total of 18 points), giving τ values ranging from 5 ms to 56 ms. The Gaussian-shaped pulse employed in frequency selection cut off at 1% of its maximum amplitude, and thus the time shift, τ_{sh}, was calculated to be 1.2 ms according to eq. [1].

$$\tau_{sh} \cong \tau_p \times 0.24 \qquad \text{eq. [1]}$$

^{13}C Transverse magnetization was generated using cross polarization with a contact time of 1.5 ms and a ^{1}H 90^{o} pulse length of 1.97 µs. The relaxation delay was set to 20 s to ensure full recovery of the magnetization during signal averaging. The spectra were collected with spectral windows of 300 ppm and a total of 8 scans, and the carrier frequency was set at the center of the two selective pulse frequencies. FIDs were zero-filled and a trapezoid window function was applied during signal processing using JEOL Delta v5.0.4.4 NMR processing software. Signal intensities were measured and normalized with respect to the reference experiment, where the intensity of the first data point of the reference was set to unity. The resulting intensity ratios of normalized *J*-modulated to reference signals (S/S_o) were plotted against the total echo interval and the resulting curve was fit to eq. [2].

$$S(\tau) = A \cos[\pi J (\tau - \tau_{sh})] \qquad \text{eq. [2]}$$

At least three measurements of the reported ^{13}C-^{13}C spin-coupling were made on each sample.

Calculations

A. Geometry Optimizations. Density functional theory (DFT) calculations were conducted on fully substituted models of methyl β-D-glucopyranoside (**3**^{k}), methyl β-lactoside (**2**^{k}) and methyl α-lactoside (**4**^{k}) within *Gaussian*09[40] using the B3LYP functional[41,42] and the 6-31G* basis set[43] (the superscript "k" denotes an *in silico* structure on which geometric optimizations were performed). In all geometry optimizations, the effects of solvent water were treated using the Self-Consistent Reaction Field (SCRF)[44] and the Integral Equation Formalism (polarizable continuum) model (IEFPCM).[45] In all calculations on **3**^{k}, the initial value of the C2–C1–O1–CH_3 torsion angle (*exo*-anomeric torsion angle[46–49]) (Scheme 3) was set at 180° and allowed to optimize during the optimization.

The effects of exocyclic C–O and C–C bond rotations on calculated $^1J_{C1,C2}$, $^2J_{C1,C3}$ and $^3J_{C1,C6}$ values in **3**^{k} were investigated by rotating the C1–C2–O2–H, C2–C3–O3–H, C3–C4–O4–H, C4–C5–C6–O6 and C5–C6–O6–H torsion angles individually from 0° to 360° in 60° increments and holding them constant during geometry optimization, giving 7776 final optimized structures. These calculations were conducted to determine the torsional dependencies of the three indicated *J*-couplings.

The dependencies of $^1J_{C1,C2}$, $^2J_{C1,C3}$ and $^3J_{C1,C6}$ in **3**^{k} on the C1–C2–O2–H and C4–C5–C6–O6 torsion angles, respectively, were determined by rotating each angle from 0° to 360° in 15° increments and holding it constant during geometry optimization. The remaining exocyclic torsion angles were allowed to optimize. Each conformer was subjected to geometry optimization, giving 24 optimized structures in each case. These calculations were performed to parameterize accurate Karplus-like relationships between the three *J*-couplings and the molecular torsion angle or angles.

For model disaccharides **2**^{k} and **4**^{k}, the *O*-glycosidic torsion angles *phi* (ϕ) (H1'–C1'–O1'–C4) and *psi* (ψ) (C1'–O1'–C4–H4) (Scheme 2) were rotated from 0° to 360° in 15° increments and held constant during geometry optimization. The remaining exocyclic C–C and C–O torsion angles in **2**^{k} and **4**^{k} were constrained as described in Scheme S2 (Supporting Information).

B. Calculations of J_{CC} *Spin-Coupling Constants.* J_{CC} spin-coupling constants were calculated in all geometry optimized structures of **2**^{k}, **3**^{k} and **4**^{k} using DFT and the B3LYP functional[41,42] in *Gaussian*09.[40] The Fermi contact,[50–52] diamagnetic and paramagnetic spin-orbit, and spin-dipole terms[50] were recovered using a specially designed basis set, [5s2p1dl3s1p],[10,53] and raw (unscaled) calculated couplings are reported and are accurate to within ± 0.2–0.3 Hz based on prior work.[13,53] The Self-Consistent Reaction Field (SCRF)[44] and the Integral Equation Formalism (polarizable continuum) model (IEFPCM)[45] were used to treat the effects of solvent water during the J_{CC} calculations.

C. J_{CC} Equation Parameterization. Equations relating DFT-calculated J_{CC} values to specific molecular torsion angles in **2**^{k}, **3**^{k} and **4**^{k} were parameterized using the scipy and numpy packages in *Python*. Equations were parameterized using J_{CC} values calculated in a sub-population of conformers that was selected using a 10 kcal/mol energy cut-off to remove a limited number of highly structurally strained conformers.[54,55] A secondary constraint was also applied when needed to remove DFT-optimized structures

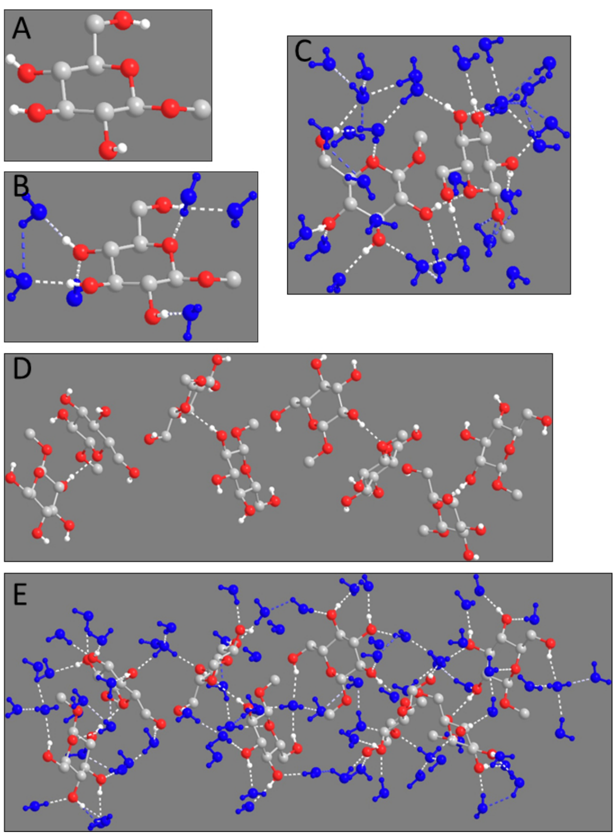

Figure 1. Models **3**^{ca}–**3**^{ce} of the crystal structure of **3** used for J_{CC} calculations (set 1). All calculations were performed on fixed conformers (i.e., no geometry optimization). (A) Model **3**^{ca} devoid of hydrogen bonding. (B) Model **3**^{cb} containing hydrogen-bonded water molecules that mimic the hydrogen bonding pattern observed in the crystal. (C) Model **3**^{cc} containing two saccharide residues with water molecules that mimic the hydrogen bonding pattern observed in the crystal. (D) Model **3**^{cd} containing eight saccharide residues with hydrogen bonding between residues observed in the crystal. (E) Model **3**^{ce} recapitulating the complete crystal structure showing hydrogen-bonded water molecules to eight saccharide residues.

containing distorted aldohexopyranosyl rings; Cremer-Pople puckering parameters were calculated from DFT-generated Cartesian coordinates and a θ value of 35^{o} was used as the cut-off.[54,55] The goodness-of-fit of each equation is reported as a root-mean-square deviation (RMSD). Equation parameterization was further evaluated using Akaike information criterion (AIC), resulting in truncated forms of two equations.

D. Fixed Structure J_{CC} Calculations. J_{CC} calculations were performed on a single fixed structure of **2**^{c}, **3**^{c} and **4**^{c} (the superscript "c" denotes an *in silico* structure in a conformation identical to that found in the crystal structure). The Cartesian coordinates for each structure were extracted from their x-ray crystal structures and used as input for J_{CC} calculations. These structures were not geometry optimized prior to the J_{CC} calculations.

For model **3**^{c}, five sets of fixed-structure J_{CC} calculations were performed. First, J_{CC} values were calculated in a single molecule of **3**^{c} in the conformation observed in its x-ray structure (Figure 1A). The J_{CC} values were then re-calculated with water molecules surrounding the single molecule to emulate the hydrogen bonding pattern observed in the x-ray crystal packing structure (Figure 1B). J_{CC} calculations were then performed on two molecules of **3**^{c} extracted from the x-ray crystal packing structure and containing a hydrogen bond between O2H (donor) of one molecule and the ring oxygen (acceptor) of the second molecule (Figure 1C). These calculations also included solvent water molecules surrounding the two molecules to emulate the hydrogen bonding pattern observed in the crystal structure. The fourth and fifth sets of

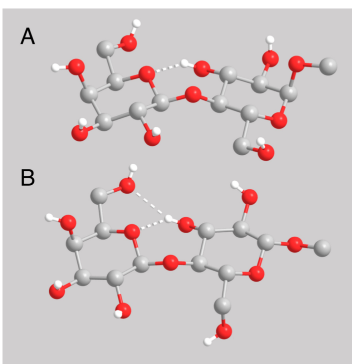

Figure 2. Model structures **4**^{c} (A) and **2**^{c} (B) used to calculate $^3J_{C1',C5}$ values by DFT (see Results and Discussion). The structures were obtained from the crystal structures of **4**$^{1',5}$ and **2**$^{1',5}$ (see text).

Table 1. Torsion Angles[a] Observed in Low-Temperature X-ray Crystal Structures of **3**^{1,3} and **3**^{1,6}.

torsion angle	compound **3**^{1,3}	compound **3**^{1,6}
C2–C1–O1–CH_3	170.57 (11)	170.52 (12)
C1–C2–O2–H	91.5 (17)	92.2 (17)
C2–C3–O3–H	174.8 (18)	174.7 (19)
C4–C5–C6–O6	–172.45 (11) (*gt* rotamer)	–172.42 (12) (*gt* rotamer)
C5–C6–O6–H	–58.5 (17)	–57.0 (17)

[a]In degrees, with errors from crystallographic analyses shown in parentheses. Values are similar but not identical to those of a prior room temperature crystal structure of **3** (ref. 31).

J_{CC} calculations included eight molecules of **3**^{c} extracted from the x-ray crystal packing structure, with and without solvent water molecules, the former emulating the hydrogen bonding pattern observed in the crystal structure (Figures 1D and 1E).

Fixed structure J_{CC} calculations were conducted on models **2**^{c} and **4**^{c} using the Cartesian coordinates associated with their x-ray crystal structures. The calculations on **2**^{c} and **4**^{c} included only atoms that comprise the disaccharide (Figure 2).

Results and Discussion

A. Low-Temperature X-Ray Crystal Structures of ^{13}*C-labeled* ***2–4****.* Low-temperature (120K) x-ray crystal structures of ^{13}C-labeled **2–4** (Scheme 3) were obtained to measure relevant torsion angles in the same crystalline samples on which solid-state ^{13}C NMR measurements would be made, and to improve the accuracy of torsion angles obtained from previously reported room temperature structures of **2** and **3**. The observed torsion angles (Tables 1 and 2) were similar but not identical to those reported previously.[31–33] Errors in torsion angles defined by heavy atoms (e.g., C2–C1–O1–CH_3 in **3**; Table 1) are ~10-times smaller (~0.2^o) than those involving hydroxyl hydrogens (~2^o) as expected; reduced electron density around hydrogen causes greater uncertainty in the locations of the hydrogens. The aldohexopyranosyl rings in the crystal structures of **3**^{1,3} and **3**^{1,6}, and those in **2**$^{1',5}$ and **4**$^{1',5}$, assume $^4C_1$ chair conformations as expected, consistent with their behaviors in aqueous (^2H_2O) solution based on inspections of intra-ring $^3J_{HH}$ values (Table S2, Supporting Information). Given the very similar crystal structure parameters obtained on

Table 2. Torsion Angles[a] Observed in Low Temperature X-ray Crystal Structures of **2**$^{1',5}$ and **4**$^{1',5}$.

torsion angle	compound	
	2$^{1',5}$	**4**$^{1',5}$
C2'–C1'–O1'–C4	153.85 (15)	148.30 (15)
O5'–C1'–O1'–C4	–88.40 (17)	–93.76 (18)
H1'–C1'–O1'–C4	31.92	25.83
C1'–O1'–C4–C3	78.19 (19)	93.74 (17)
C1'–O1'–C4–C5	–162.13 (14)	–144.75 (14)
C1'–O1'–C4–H4	–44.17	–27.54
O5–C5–C6–O6	–54.80 (19) (*gg* rotamer)	72.6 (2) (*gt* rotamer)

[a]In degrees, with errors from crystallographic analyses shown in parentheses. Data for **2**$^{1',5}$ and **4**$^{1',5}$ were obtained in this work, but are very similar to those obtained from prior crystal structures (refs. 32–33).

$\mathbf{3}^{1,3}$ and $\mathbf{3}^{1,6}$ (Table 1), similar parameters were assumed in the crystal structure of $\mathbf{3}^{1,2}$ and its x-ray structure was not determined.

*B. Conformational Factors That Influence J_{CC} Values in ^{13}C-Labeled **2–4** and Core Questions in This Study.* For $^{1}J_{C1,C2}$ in $\mathbf{3}^{1,2}$, coupling magnitude depends mainly on conformations about the C1–O1 (ϕ) and C2–O2 bonds (Scheme 4A).[11] $^{2}J_{C1,C3}$ in $\mathbf{3}^{1,3}$ depends mainly on conformation about the C2–O2 bond, with secondary dependencies on the conformations about the C1–O1 (ϕ) and C3–O3 bonds (Scheme 4B).[9] $^{3}J_{C1,C6}$ in $\mathbf{3}^{1,6}$ depends mainly on the endocyclic C1–O5–C5–C6 torsion angle,[12,13,35] which is constrained to ~180° by the ring, with a secondary dependence on conformation about the C5–C6 bond (ω; exocyclic hydroxymethyl conformation) (Scheme 4C).[13] The latter secondary dependence reflects the terminal electronegative substituent effect[14,35] from O6, whose magnitude depends on the rotation about ω. The $^{1}J_{CC}$, $^{2}J_{CCC}$ and $^{3}J_{COCC}$ values between the ^{13}C-labeled carbons in $\mathbf{3}^{1,2}$, $\mathbf{3}^{1,3}$ and $\mathbf{3}^{1,6}$, respectively, have positive signs regardless of the conformational contributions to their magnitudes.[56,57] In solution, time-averaging of the above-noted conformational factors contributes to experimental $^{1}J_{C1,C2}$, $^{2}J_{C1,C3}$ and $^{3}J_{C1,C6}$ values in **3** in a complex manner, making their quantitative interpretation in conformational terms difficult. The latter accrues because, unless these contributions can be properly accounted for in DFT calculations of these J_{CC} values, and they often cannot, it is not possible to use DFT-calculated J_{CC} values to help interpret the

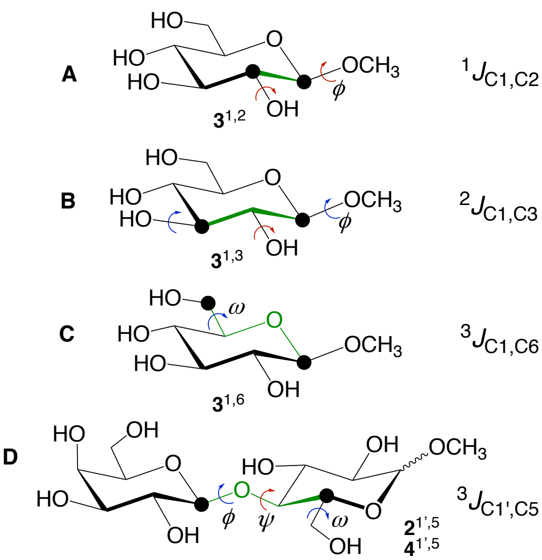

Scheme 4. Conformational determinants of J_{CC} values. A) $^{1}J_{C1,C2}$ in $\mathbf{3}^{1,2}$. B) $^{2}J_{C1,C3}$ in $\mathbf{3}^{1,3}$. C) $^{3}J_{C1,C6}$ in $\mathbf{3}^{1,6}$. D) $^{3}J_{C1',C5}$ in $\mathbf{2}^{1',5}$ and $\mathbf{4}^{1',5}$. Coupling pathways are shown in green. Curved arrows in red identify major determinants of the indicated coupling. Curved arrows in blue identify minor determinants of the indicated coupling. Black circles denote the coupled (^{13}C-labeled) carbons. See text for explanations.

experimental values measured in solution, or to establish whether DFT-calculated J_{CC} values are quantitative. However, this time-averaging is eliminated in crystalline samples, allowing DFT-calculated J_{CC} values to be determined in single conformers, and comparisons of these calculated values made to experimental J_{CC} values measured in the same conformers. The latter comparison provides a suitable means of determining whether DFT-calculated J_{CC} values are quantitative.

The three-bond (vicinal) trans-glycosidic *J*-couplings between C1' and C5 in $\mathbf{2}^{1',5}$ and $\mathbf{4}^{1',5}$ exhibit primary Karplus-like dependencies on the C1'–O1'–C4–C5 torsion angle (Scheme 4D).[14,35,54,55] Secondary effects arise from rotations of the C1'–O1' (ϕ) and the C5–C6 bonds (ω). The presence of O5 as a terminal in-plane electronegative substituent also affects the behavior of $^3J_{C1',C5}$ (Scheme 4D).[14] Recent NMR studies of redundant trans-glycosidic *J*-couplings using *MA'AT* analysis have shown that the preferred values of ψ in **2** and **4** in aqueous solution are essentially identical (mean C1'–O1'–C4–H4 torsion angles of –8.0°).[54] In contrast, significantly different ψ values are observed in crystalline $\mathbf{2}^{1',5}$ and $\mathbf{4}^{1',5}$, as determined by comparing corresponding C1'–O1'–C4–C3 and C1'–O1'–C4–C5 torsion angles (Table 2). A key question in the present study is whether the ~17° difference that exists between the two crystalline samples can be detected quantitatively by $^3J_{C1',C5}$ values measured in crystalline $\mathbf{2}^{1',5}$ and $\mathbf{4}^{1',5}$.

Table 3. Experimental and Calculated ^{13}C-^{13}C Spin-Coupling Constants in ^{13}C-Labeled **2**–**4**.

cmpd	J_{CC}	solid-state ^{13}C NMR[a] (Hz)	solution $^{13}C\{^1H\}$ NMR[b] (Hz)	DFT-calculated J_{CC} (Hz)[e]	
				crystal	Karplus eq.
$\mathbf{3}^{1,2}$	$^1J_{C1,C2}$	49.1	46.8	46.8[f]	49.9
$\mathbf{3}^{1,3}$	$^2J_{C1,C3}$	5.2[c]	(+) 4.6	(+) 6.4[f]	(+) 5.9
$\mathbf{3}^{1,6}$	$^3J_{C1,C6}$	3.9	4.1	3.5[f]	4.2
$\mathbf{2}^{1',5}$	$^3J_{C1',C5}$	4.8[d]	2.1	5.1	5.1
$\mathbf{4}^{1',5}$	$^3J_{C1',C5}$	4.0	2.0	4.1	4.1

[a]Solid-state experimental *J*-couplings have a 95% confidence interval of ±0.2 Hz for $^1J_{CC}$ and ±0.1 Hz for $^2J_{CCC}$ and $^3J_{COCC}$ (n = 6). [b]Experimental errors for solution *J*-couplings are ±0.1 Hz; values were measured at ~22 °C in ^2H_2O. [c]The sign of $^2J_{CCC}$ in $\mathbf{3}^{1,3}$ measured by solid-state ^{13}C NMR was not determined experimentally; the absolute value is shown. [d]Value was obtained in the presence of overlapping signals and may be less accurate. [e]See text for discussion of how these J_{CC} values were calculated. [f]Average values obtained from DFT calculations on $\mathbf{3}^{ce}$.

*C. ^{13}C-^{13}C Spin-Couplings in ^{13}C-Labeled **2–4** in Solution and in Crystalline Samples.* High-resolution $^{13}C\{^1H\}$ NMR spectra of ^{13}C-labeled **2–4** were obtained in aqueous (^2H_2O) solution, and ^{13}C-^{13}C spin-couplings between the ^{13}C-labeled carbons were extracted from each doublet in the spectra (Figures S1–S5, Supporting Information) (Table 3). J_{CC} values so obtained on **3** were identical to those reported previously;[13] $^3J_{C1',C5}$ values measured in $\mathbf{2}^{1',5}$ and $\mathbf{4}^{1',5}$ were identical, as reported previously.[54]

Cross-polarization magic angle spinning 1D ^{13}C NMR spectra of ^{13}C-labeled **2–4** contained strong signals arising from the ^{13}C-labeled carbons (Figure 3). Signal splitting caused by ^{13}C-^{13}C spin-coupling caused by $^1J_{C1,C2}$ was observed only in the spectrum of $\mathbf{3}^{1,2}$; resonance line-widths (~30 Hz) precluded the observation of line splitting from the much smaller $^2J_{CC}$ and $^3J_{CC}$ values in spectra of $\mathbf{3}^{1,3}$, $\mathbf{3}^{1,6}$, $\mathbf{2}^{1',5}$ and $\mathbf{4}^{1',5}$. Signal intensities in *J*-modulated (*S*) and reference (S_o) spectra were measured as a function of τ (Figures 4A–E), and plots of the ratio, S/S_o, *vs* τ were fit to eq. [2] (Figures 4F–J). The fitting statistics from multiple experiments are given in Table S3 of the Supporting Information. ^{13}C-^{13}C *J*-couplings measured in crystalline samples of $\mathbf{3}^{1,2}$ and $\mathbf{3}^{1,3}$ were found to differ significantly from corresponding values measured in aqueous solution. Specifically, a 2.3 Hz difference was observed for $^1J_{C1,C2}$ and a 0.6 Hz difference was observed for $^2J_{C1,C3}$ (Table 3). In contrast, $^3J_{C1,C6}$ values measured in $\mathbf{3}^{1,6}$ in solution

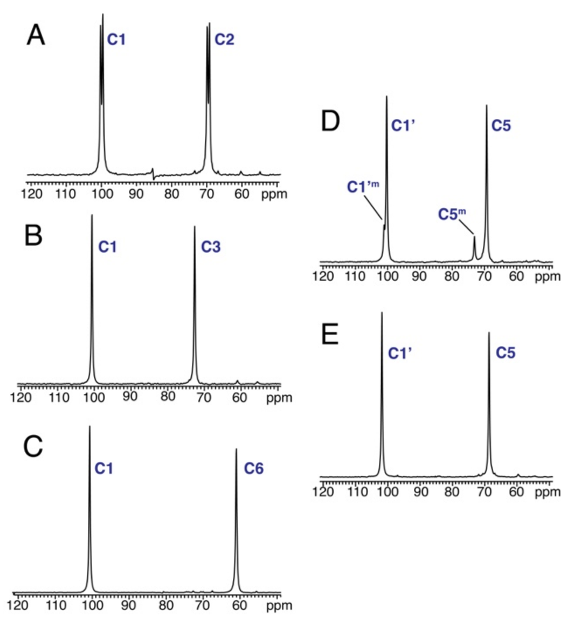

Figure 3. Cross-polarization magic-angle spinning (CP-MAS) 1D $^{13}C\{^1H\}$ NMR spectra (75 MHz) of $\mathbf{3}^{1,2}$ (A), $\mathbf{3}^{1,3}$ (B), $\mathbf{3}^{1,6}$ (C), $\mathbf{2}^{1',5}$ (D), and $\mathbf{4}^{1',5}$ (E), showing signal assignments. Only signals arising from ^{13}C-labeled carbons are shown. In (D), signals from a minor crystalline form of **2** are identified with "m" superscripts.

and in crystalline samples were very similar (Table 3); the ~0.2 Hz difference lies within the error of the measurements.

$^3J_{C1',C5}$ values in $\mathbf{2}^{1',5}$ and $\mathbf{4}^{1',5}$ depend strongly on *psi* (ψ) (Scheme 4D)[9,14,35,54] and are essentially identical when measured in aqueous solution (2.0 – 2.1 Hz) (Table 3). These values differ significantly, however, when measured in crystalline samples; $^3J_{C1',C5}$ is 4.8 Hz in $\mathbf{2}^{1',5}$ and 4.0 Hz in $\mathbf{4}^{1',5}$ (Table 3). In addition, $^3J_{C1',C5}$ values measured in aqueous solutions of $\mathbf{2}^{1',5}$ and $\mathbf{4}^{1',5}$ and those measured in crystalline samples differ by 2 – 3 Hz (Table 3).

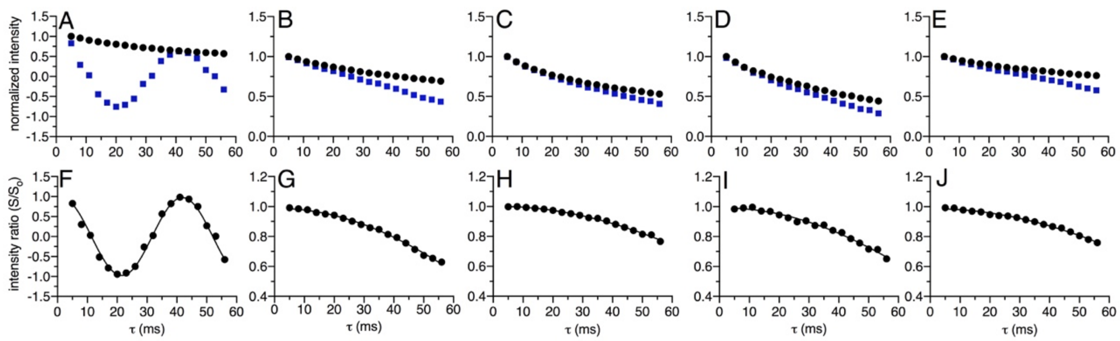

Figure 4. Measurements of $^1J_{C1,C2}$ (A and F), $^2J_{C1,C3}$ (B and G), $^3J_{C1,C6}$ (C and H), $^3J_{C1',C5}$ (D and I), and $^3J_{C1',C5}$ (E and J) in $\mathbf{3}^{1,2}$, $\mathbf{3}^{1,3}$, $\mathbf{3}^{1,6}$, $\mathbf{2}^{1',5}$ and $\mathbf{4}^{1',5}$, respectively. The detected spins were C2, C1, C6, C1' and C5 from left to right. (A–E). Normalized intensities of the *J*-modulated echo signals (*S*; blue points) and the reference echo signals (S_0; black points) plotted against the total echo interval, τ. (F–J) Intensity ratios, S/S_0, plotted against τ. The solid lines represent the best fits to eq. [1]. All experiments were run in triplicate, and only one representative signal is shown for each compound.

X-ray analyses of crystalline $\mathbf{2}^{1',5}$ and $\mathbf{4}^{1',5}$ reveal a single conformation in their crystal lattices. No evidence of conformational heterogeneity is observed, unlike the behavior of other disaccharides.[58–59] The solid-state ^{13}C NMR spectrum of $\mathbf{4}^{1',5}$ contains a single pair of signals indicative of a single conformation in the crystal as expected (Figure 3E). However, two pairs of signals were observed in the solid-state ^{13}C NMR spectrum of $\mathbf{2}^{1',5}$ (Figure 3D), and crystallization of multiple samples of $\mathbf{2}^{1',5}$ failed to eliminate the minor signals or change the relative abundances of the two pairs. The ratio of minor to major signals remained relatively constant at ~1:10. This observation of minor signals suggests that two different types of crystals coexist in the sample, each containing a different conformation of **2**$^{1',5}$. In contrast to ssNMR analysis, which involves bulk sampling, single crystals are used for X-ray analysis such that the presence of two different crystalline forms of **2**$^{1',5}$ would be detected only if a statistically significant number of crystals was analyzed, which was not undertaken. Furthermore, a visual examination of crystalline samples of **2**$^{1',5}$ by light microscopy failed to reveal two different crystalline morphologies. However, experimental evidence supporting the proposition that the weak signals arise from another crystalline form of **2**$^{1',5}$ was obtained by measuring the $^{3}J_{C1',C5}$ value in this species. The value of 4.7 ± 0.1 Hz is nearly identical to that observed in the dominant crystalline form of **2**$^{1',5}$ (Table 3), suggesting that the two crystalline forms have very similar, if not identical, ψ torsion angles. The slightly different ^{13}C chemical shifts in the two forms might be caused by other structural differences such as different ϕ torsion angles, exocyclic hydroxymethyl group conformations, exocyclic C–O bond torsion angles, and/or intra- or intermolecular hydrogen bonding interactions in the crystalline lattice.

*D. Quantitative Comparisons of Calculated J_{CC} Values in **2–4** to Experimental J_{CC} Values Measured in Crystalline ^{13}C-Labeled **2–4**.* Two sets of DFT calculations were collected to determine whether calculated J_{CC} values in **3**, and by extension **2** and **4**, can be compared quantitatively to corresponding experimental J_{CC} values measured in crystalline **2**$^{1',5}$, **3**^{1,2}, **3**^{1,3}, **3**^{1,6} and **4**$^{1',5}$. The first set (Set 1; see Calculations, Part D) was performed on **3**^{c} in the same conformation observed in the crystal structure of **3** in five different states of solvation (denoted **3**^{ca}–**3**^{ce}) that recapitulate, to varying degrees, the intermolecular interactions observed in the crystal lattice (Figure 1). The variables in these calculations were the number of **3**^{c} molecules employed in the model and the nature of the solvation (i.e., hydrogen bonding) shell. The second set (Set 2; see Calculations, Parts A–C) involved rotating specific torsion angles in **3**^{k}, followed by geometry optimizations, to produce a set of conformers in which specific J_{CC} values were subsequently calculated and used to parameterize equations that relate each J_{CC} to a particular torsion angle. Calculations of this type have been used recently to determine population distributions of saccharide conformers in solution.[54,55] Parameterized equations obtained in this manner have been difficult to validate experimentally, and the present work sought this validation by measuring J_{CC} values in conformationally constrained (crystalline) samples.

The DFT calculations in Set 1 (Figure 1) were used to determine whether the unique properties of crystalline solids such as crystal packing forces and long-range electrostatics significantly affect calculated J_{CC} values. These calculations showed that solid-state properties exert a negligible effect on calculated J_{CC} values (Table 4), at least as manifested in five different crystal models of **3**^{c} (Figure 1). An alternate computational method, CASTEP[60–62], has been described that presumably takes these properties into account when calculating NMR *J*-couplings in solids, but several of its features rendered it unattractive for the present work. Evaluating the accuracy of DFT-calculated J_{CC} values was the prime focus of this work, rather than demonstrating that J_{CC} values can be calculated in solids using established methods (e.g., CASTEP) without regard for accuracy. In addition, because accuracy was of prime concern, J_{CC} values were calculated using a basis set[10,52] specifically tailored to treat saccharides. It is unlikely that CASTEP will yield more accurate J_{CC} values since it is not tailored to saccharides. Consequently, using CASTEP would undermine the key objective of the work. Finally, calculating *J*-couplings in a crystal structure using CASTEP is normally performed in two steps. The hydrogen atoms in the crystal structure are relaxed, and *J*-couplings are then calculated on the relaxed structure. While this approach is useful for low-resolution crystal structures, the high-resolution (low-temperature) crystal structures used in this work allowed free

Table 4. J_{CC} Values[a] Calculated by DFT in Five Models[b], **3**^{ca}–**3**^{ce}, of the Crystal Structure of **3**.

J-coupling	calculated J_{CC} values				
	3^{ca}	**3**^{cb}	**3**^{cc} (average)	**3**^{cd} (average)	**3**^{ce} (average)
$^{1}J_{C1,C2}$	47.2	46.6	46.6	47.0	46.8
$^{2}J_{C1,C3}$	6.8	6.5	6.4	6.9	6.4
$^{3}J_{C1,C6}$	3.6	3.5	3.6	3.6	3.5

[a]In Hz. [b]See Figure 1 for the definitions of these models.

refinement of the polar hydrogen atoms yielding precise determinations, eliminating the need for hydrogen atom relaxation. More importantly, hydrogen positions are particularly relevant to two of the five J_{CC} values studied, namely, $^{1}J_{C1,C2}$ and $^{2}J_{C1,C3}$ in $\mathbf{3}^{1,2}$ and $\mathbf{3}^{1,3}$, respectively. Relaxing hydrogens in the crystal structure conformation of $\mathbf{3}^{c}$ could adversely affect molecular torsion angles involving hydrogens, leading to significant errors in calculated J_{CC} values. This complication does not pertain to vicinal $^{3}J_{COCC}$ values in $\mathbf{3}^{1,6}$, $\mathbf{2}^{1',5}$ and $\mathbf{4}^{1'5}$, whose magnitudes are almost exclusively determined by the C–O–C–C torsion angle[14,35] (Scheme 4) and are minimally affected by hydrogen atom disposition relative to the coupling pathway. Taken collectively, these limitations render CASTEP unreliable as a tool to calculate J_{CC} values in $\mathbf{3}^{c}$, and by extension in $\mathbf{2}^{c}$ and $\mathbf{4}^{c}$, that can be compared quantitatively to experimental J_{CC} values measured in crystalline samples.

The DFT calculations in Set 1 demonstrate that solid-state properties exert only very small effects on calculated J_{CC} values in $\mathbf{3}^{c}$, that is, calculated J_{CC} values for the structures shown in Figure 1 were very similar (Table 4). Given this finding, model $\mathbf{3}^{k}$ (see Supporting Information for Cartesian coordinates) was used to generate parameterized equations that relate specific J_{CC} values to specific torsion angles. These calculations were conducted with the inclusion of a solvent continuum model (see Calculations, Part B), as well as *in vacuo* and with various other solvent models (data not shown), with only very small differences in

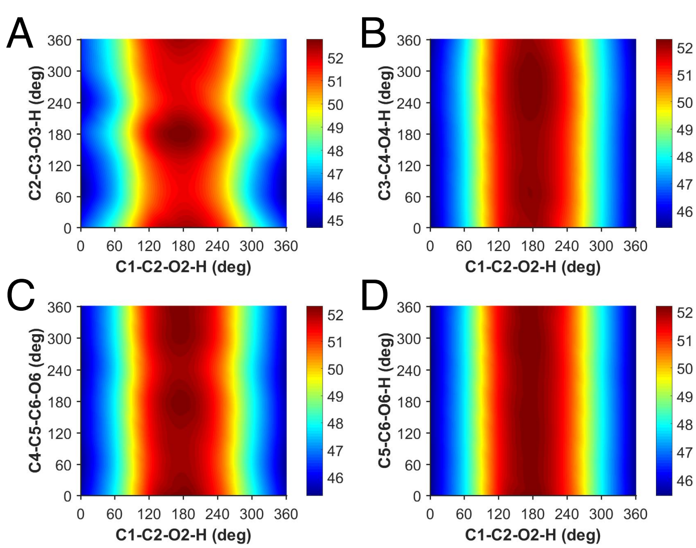

Figure 5. 2D Contour plots of calculated $^{1}J_{C1,C2}$ values in $\mathbf{3}^{k}$ showing a primary dependence on the C1–C2–O2–H torsion angle (*x*-axes) and secondary effects of rotating the C3–O3 (A), C4–O4 (B), C5–C6 (C) and the C6–O6 (D) bonds (*y*-axes) on this dependency.

calculated J_{CC} values observed between these treatments. Importantly, calculated J_{CC} values obtained from the resulting parameterized equations (Set 2) were in much better agreement with J_{CC} values measured in crystalline samples than were J_{CC} values calculated from single conformers of **3**^{ca}–**3**^{ce} (Set 1) that replicate the crystal structure of **3**. The better accuracy of the parameterized equations probably evolves from the fact that these equations are derived from a relatively large set of conformers, resulting in an "error-averaged" equation. This presumed cancellation of systematic error gives equations that capture the torsional dependencies of J_{CC} values with greater accuracy than what is achievable using a single crystal structure conformer of **3**^{c}.

The DFT calculations on **3**^{k} in Set 2 included one structure constraint on the C2–C1–O1–CH_3 torsion angle. This angle was set initially at ~180°, which is known to be highly preferred in aqueous solution due to stereoelectronic factors (*exo*-anomeric effect).[46–49] Consequently, since rotational averaging about the C1–O1 bond is expected to be minimal in solution, the effect of this rotation on calculated J_{CC} values in **3**^{k} was not investigated. The initial C2–C1–O1–CH_3 torsion angle was allowed to optimize, however, and consistently gave optimized values of 165–172°. The effects of all remaining exocyclic bond rotations in **3**^{k} (i.e., C2–O2, C3–O3, C4–O4, C5–C6 and C6–O6 bonds) on calculated J_{CC} values were investigated.

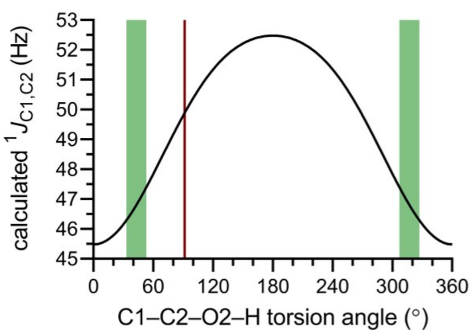

Figure 6. Calculated $^{1}J_{C1,C2}$ values in **3**^{k} as a function of the C1–C2–O2–H torsion angle described by eq. [3] (black curve). The red line corresponds to the torsion angle observed in the crystal structure of **3**. The green lines correspond to predicted mean positions of torsion angle distributions based on the $^{1}J_{C1,C2}$ value measured in aqueous solution.

*E. $^{1}J_{C1,C2}$ in **3**^{k} and **3**^{1,2}.* Contour plots of calculated $^{1}J_{C1,C2}$ values in **3**^{k} were used to visualize the effects of exocyclic C–O and C–C bond conformations on this *J*-value (Figure 5). $^{1}J_{C1,C2}$ exhibited a dynamic range of ~7 Hz due almost exclusively to the effect of rotation of the C2–O2 bond, being essentially unaffected by rotation of the C4–O4, C5–C6 and C6–O6 bonds. A small effect from rotation of the C3–O3 bond is observed (Figure 5A). These findings are consistent with prior work[11] showing that $^{1}J_{CX,CY}$ values in HO–C_x–C_y–OH fragments depend strongly on conformation about the C–C bond and about the two C–O bonds involving the coupled carbons, with the latter effects often stronger than the former. In $\mathbf{3}^{k}$, conformations about the C1–O1 and C1–C2 bonds are constrained (the former by the *exo*-anomeric effect[46–49] and the latter by the relatively rigid pyranosyl ring), so that only conformation about the C2–O2 bond remains a major determinant.

The dependence of $^{1}J_{C1,C2}$ on the C1–C2–O2–H torsion angle θ in $\mathbf{3}^{k}$ was parameterized to give eq. [3], whose function is plotted in Figure 6 (black line).

$$^{1}J_{C1,C2}\ (\mathrm{Hz}) = 49.39 - 3.50\cos(\theta) - 0.41\cos(2\theta)$$
$$\mathrm{RMSD} = 0.19\ \mathrm{Hz} \qquad \text{eq. [3]}$$

In crystalline $\mathbf{3}^{1,2}$, the C1–C2–O2–H torsion angle is 92 ± 2° (Table 1), which correlates with a $^{1}J_{C1,C2}$ value of 49.9 Hz based on eq. [3] (Figure 6, Table 3). This value is very similar to that measured in crystalline $\mathbf{3}^{1,2}$ (49.1 ± 0.2 Hz) (Table 3), confirming the accuracy of eq. [3]. The difference (~0.8 Hz) is statistically insignificant given the RMSD of eq.[3] and the error in the experimental value of $^{1}J_{C1,C2}$.

$^{1}J_{C1,C2}$ in $\mathbf{3}^{1,2}$ measured in aqueous solution (46.8 Hz) differs significantly from that measured in the solid (49.1 Hz) (Table 3). The smaller value in solution suggests that conformers of **3** having C1–C2–O2–H torsion angles with mean positions of approximately +45° and/or –45° are highly preferred (Figure 6). Future work will test this model experimentally through *MA'AT* analysis of redundant *J*-couplings that are sensitive to C2–O2 bond torsions.[9,63]

F. $^{2}J_{C1,C3}$ *in* $\mathbf{3}^{k}$ *and* $\mathbf{3}^{1,3}$*.* 2D contour plots of calculated $^{2}J_{C1,C3}$ values in $\mathbf{3}^{k}$ show dynamic ranges of ~4 Hz and a strong dependence on the C1–C2–O2–H torsion angle (Figure 7).[9] Rotations of the C4–O4, C5–C6 and C6–O6 bonds (Figure 7B–D) do not affect $^{2}J_{C1,C3}$ appreciably, while a minor effect (± 0.4 Hz) is observed from rotation of the C3–O3 bond (Figure 7A).

The dependence of $^{2}J_{C1,C3}$ on the C1–C2–O2–H torsion angle θ in $\mathbf{3}^{k}$ was parameterized to give eq. [4], whose function is plotted in Figure 8.

$$^{2}J_{C1,C3}\ (\text{Hz}) = 5.31 + 0.19\cos(\theta) - 0.21\sin(\theta) - 0.78\cos(2\theta) - 1.27\sin(2\theta)$$

RMSD = 0.10 Hz eq. [4]

The value of $^{2}J_{C1,C3}$ predicted from eq. [4] at the C1–C2–O2–H torsion angle of 91.5 ± 2^{o} observed in crystalline **3** (Table 1) is +5.9 Hz (Figure 8), which is similar to that measured experimentally in crystalline $\mathbf{3}^{1,3}$ (5.2 Hz; Table 3). The relatively good agreement between the calculated and experimental values provides new experimental evidence supporting the calculated dependence of $^{2}J_{C1,C3}$ on conformation about the C2–O2 bond. A parameterized equation describing the dependencies of $^{2}J_{C1,C3}$ on both the C1–C2–O2–H and C2–C3–O3–H torsion angles is expected to reduce the difference between the calculated and experimental $^{2}J_{C1,C3}$ to < 0.7 Hz.

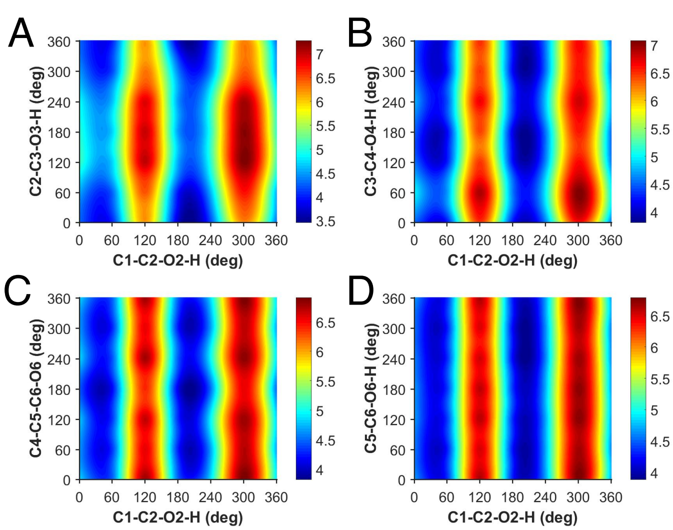

Figure 7. Contour plots of DFT-calculated $^{2}J_{C1,C3}$ values in $\mathbf{3}^{k}$ showing a primary on dependence the C1–C2–O2–H torsion angle and the effects on this dependency of rotating the C3–O3 (A), C4–O4 (B), C5–C6 (C) and the C6–O6 (D) bonds.

The above interpretation of $^1J_{C1,C2}$ in $\mathbf{3}^{1,2}$ measured in aqueous solution led to a proposed model in which the C1–C2–O2–H torsion angle assumes mean values of ± 45° (Figure 6). At –45° (315°), a value of 6.6 Hz is calculated from eq. [4], which is significantly larger than the experimental value (4.6 Hz) (Table 3). On the other hand, at 45°, eq. [4] yields a $^2J_{C1,C3}$ value of 3.9 Hz, in closer agreement with the experimental value, suggesting that a mean position of the torsion angle near 45° is preferred. In this geometry, O2H is approximately *anti* to C3, with O3<u>H</u> pointing towards O1 in an orientation potentially stabilized by intramolecular hydrogen bonding.

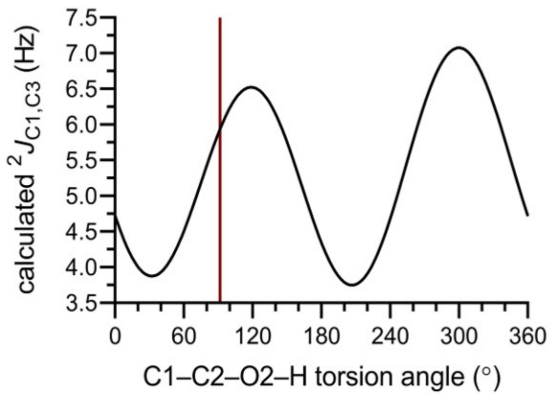

Figure 8. Calculated $^2J_{C1,C3}$ values in $\mathbf{3}^k$ as a function of the C1–C2–O2–H torsion angle. The black curve describes eq. [4]. The red line corresponds to the torsion angle observed in the crystal structure of **3**.

G. $^3J_{C1,C6}$ in $\mathbf{3}^k$ and $\mathbf{3}^{1,6}$. The magnitude of $^3J_{C1,C6}$ in $\mathbf{3}^{1,6}$ is determined mainly by the C1–O5–C5–C6 torsion angle.[13,35] However, since this angle is highly constrained at ~180° in the favored $^4C_1$ conformation of the pyranosyl ring, exocyclic hydroxymethyl group conformation (i.e., rotation about the exocyclic C5–C6 bond) becomes a key determinant of $^3J_{C1,C6}$ in solution.[12,13] This secondary dependence is evident in DFT calculations on $\mathbf{3}^k$ (Figure 9); rotation of the C2–O2, C3–O3, C4–O4 and C6–O6 bonds exerts little or no effect on $^3J_{C1,C6}$ magnitude and sign (see contour plots in Figure S6, Supporting Information). The DFT-calculated dependence of $^3J_{C1,C6}$ on the C4–C5–C6–O6 torsion angle ω was parameterized to give eq. [5].

$$^3J_{C1,C6}\text{ (Hz)} = 4.86 + 0.76\cos(\omega) - 0.76\sin(\omega) \qquad \text{RMSD} = 0.09\text{ Hz} \qquad \text{eq. [5]}$$

The value of ω in the crystal structure of $\mathbf{3}^{1,6}$ (–172.42º ± 0.12º or 187.6º ± 0.12º) (Table 1) correlates with a $^{3}J_{C1,C6}$ value of 4.2 Hz based on eq. [5] (Figure 9, Table 3). The experimental $^{3}J_{C1,C6}$ measured in crystalline $\mathbf{3}^{1,6}$ is 3.9 Hz (Table 3), a value in very good agreement with the calculated coupling when errors are considered. The experimental $^{3}J_{C1,C6}$ measured in aqueous solution is 4.1 Hz (Table 3), suggesting that ω values of ~75º (*gg* rotamer) and/or ~180º (*gt* rotamer) are highly preferred. This conclusion is consistent with prior determinations of ω that show the *gt* and *gg* rotamers to be favored in **3** in aqueous solution.[53,64]

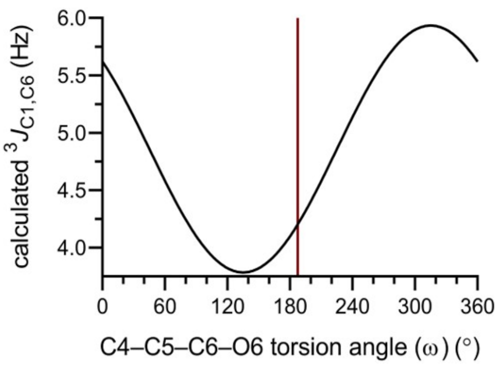

Figure 9. Calculated $^{3}J_{C1,C6}$ values in $\mathbf{3}^{k}$ as a function of the C4–C5–C6–O6 torsion angle ω. The black curve describes eq. [5]. The red line corresponds to the torsion angle observed in the crystal structure of **3** (*gt* rotamer).

H. $^{3}J_{C1',C5}$ in $\mathbf{2}^{k}$ and $\mathbf{4}^{k}$, and in $\mathbf{2}^{1',5}$ and $\mathbf{4}^{1',5}$. Trans-glycosidic $^{3}J_{C1',C5}$ values in $\mathbf{2}^{1',5}$ and $\mathbf{4}^{1',5}$ depend primarily on glycosidic torsion angle, *psi* (ψ) (Schemes 2 and 4).[14,35,54] Model structures $\mathbf{2}^{c}$ and $\mathbf{4}^{c}$ (Figure 2) devoid of the intermolecular hydrogen bonds observed in crystal structures of $\mathbf{2}^{1',5}$ and $\mathbf{4}^{1',5}$ were used in DFT calculations since the inclusion of these bonds had little effect on calculated J_{CC} values (data not shown). DFT calculations on model structures $\mathbf{2}^{k}$ and $\mathbf{4}^{k}$ allowed ψ (defined as the C1'–O1'–C4–H4 torsion angle) to be rotated in 15º increments through 360º, giving 576 geometrically optimized structures in which $^{3}J_{C1',C5}$ values were calculated. The resulting plots of $^{3}J_{C1',C5}$ *vs* ψ (Figure S7, Supporting Information) were virtually superimposable, allowing the two datasets to be combined to give parameterized eq. [6].

$$^{3}J_{C1',C5}\ (\text{Hz}) = 2.02 + 0.47\cos(\psi) - 0.63\sin(\psi) - 0.90\cos(2\psi) - 2.33\sin(2\psi)$$

$$\text{RMSD} = 0.71\ \text{Hz} \qquad \text{eq. [6]}$$

Eq. [6] was found to be in very good agreement with previous generalized parameterizations of $^3J_{C1',C5}$ in β-(1→4) linked disaccharides (Figure S7, Supporting Information).[54]

Identical $^3J_{C1',C5}$ values are observed in **2**$^{1',5}$ and **4**$^{1',5}$ (2.0 – 2.1 Hz) in aqueous solution (Table 3), and recent *MA'AT* analyses gave mean values of ψ (defined as C1'–O1'–C4–H4) of –8.0° in both disaccharides, indicating nearly identical conformations.[54] In contrast, significantly different $^3J_{C1',C5}$ values are observed in **2**$^{1',5}$ (4.8 Hz ± 0.1 Hz) and **4**$^{1',5}$ (4.0 ± 0.1 Hz) in crystalline solids (Table 3), indicating different ψ conformations in the two crystal structures, and different ψ conformations in solution and in the crystalline solids. The crystal structure of **2**$^{1',5}$ yields a ψ of –44.2° (Table 2), for which eq. [6] predicts a $^3J_{C1',C5}$ value of 5.1 Hz (Table 3, Figure 10). This calculated value of $^3J_{C1',C5}$ is very similar to the 4.8 Hz value measured in crystalline **2**$^{1',5}$. In contrast, the x-ray structure of **4**$^{1',5}$ yields a ψ of –27.5° (Table 2), for which eq. [6] predicts a $^3J_{C1',C5}$ value of 4.1 Hz (Table 3, Figure 10). The experimental $^3J_{C1',C5}$ in crystalline **4**$^{1',5}$ (4.0 Hz; Table 3) agrees well with this predicted value.

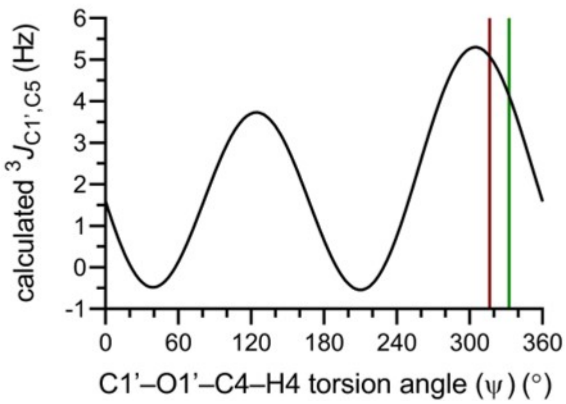

Figure 10. Calculated $^3J_{C1',C5}$ values in **2**^{k} and **4**^{k} as a function of the C1'–O1'–C4–H4 torsion angle (ψ). The red and green lines correspond to ψ values observed in the crystal structures of **2**$^{1',5}$ and **4**$^{1',5}$, respectively.

Calculated $^3J_{C1',C5}$ values in the single molecule models **2**^{c} and **4**^{c}, devoid of hydrogen bonds, are very similar to the experimental $^3J_{C1',C5}$ values determined in crystalline **2**$^{1',5}$ and **4**$^{1',5}$, in contrast to the behavior of $^1J_{C1,C2}$, $^2J_{C1,C3}$ and $^3J_{C1,C6}$ in **3**. This difference probably stems from the fact that $^3J_{C1',C5}$ depends very heavily on the C1'–O1'–C4–C5 torsion angle, with other structural factors contributing negligibly to its magnitude, rendering the need for cancellation of systematic errors, brought about through equation parameterization, less important in treating this *J*-value quantitatively.

Conclusions

The use of redundant NMR *J*-couplings to derive continuous conformational models of flexible elements in saccharides (*MA'AT* analysis[54,55]) depends on reliable DFT-calculated J_{CH} and J_{CC} values from which parameterized equations relating their values to molecular torsion angles can be obtained. While prior work has tested the reliability of these calculations, direct experimental approaches are needed to validate the computations. The present work makes use of solid-state ^{13}C NMR spectroscopy as a tool to obtain this validation. The attractiveness of the method lies in the physical nature of the sample. Crystalline saccharides have significantly reduced flexibility relative to their behaviors in solution by virtue of precise packing in the crystalline lattice. Since the precise overall conformations of saccharides can be determine by crystallography on crystalline samples, J_{CC} values measured in these samples can be directly correlated with specific and known molecular torsion angles. Contributions to J_{CC} values made by conformational exchange in solution are thereby eliminated. One drawback of the approach is the need to introduce two ^{13}C-labeled carbons into the sample site-specifically, but current synthetic techniques are robust enough to permit this labeling in most cases.

The agreement between DFT-calculated $^1J_{CC}$, $^2J_{CC}$ and $^3J_{CC}$ values and those measured by solid-state ^{13}C NMR is remarkable, attesting to (a) the accuracy of the DFT calculations and (b) the reliability of solid-state ^{13}C NMR in measuring J_{CC} values in crystalline samples. The observed sensitivity of the J_{CC} measurements is noteworthy. For example, the ψ torsion angles in methyl α-lactoside (**4**) and methyl β-lactoside (**2**) are essentially identical in aqueous solution, as shown by *MA'AT* analysis.[14] However, in their crystalline forms, these angles differ significantly from one another and from those observed in aqueous solution. As expected, the experimental $^{3}J_{C1',C5}$ values in **2** and **4** in crystalline samples differ significantly, and importantly, are in very good agreement with those predicted by DFT using models that replicate the conformations found in crystalline samples. These findings provide evidence that the various conformational dependencies of J_{CC} values in saccharides can be fruitfully interrogated by solid-state ^{13}C NMR, especially those associated with exocyclic C–O (hydroxyl groups) and C–C (exocyclic hydroxymethyl groups) bonds.

One of the shortcomings of this work is the fact that only single points were used to interrogate DFT-derived continuous functions. While the current results support the conclusion that DFT provides near quantitative calculated J_{CC} values in saccharides, complete validation awaits more extensive sampling across full torsional itineraries. Efforts to achieve the latter sampling are underway.

Although the work reported herein was performed on crystalline samples, crystallinity does not appear to be a requirement to measure J_{CC} values. *J*-Couplings have been measured and interpreted in disordered or amorphous solids.[28,65–67] Thus, solid-state ^{13}C NMR should provide accurate J_{CC} values in non-crystalline samples. This feature may prove attractive, for example, in studies of receptor-saccharide complexes that cannot be crystallized for study by conventional x-ray analysis. In this case, a set of different doubly ^{13}C-labeled ligands could be used to collect sufficient torsional information to assign bound ligand conformation.

Acknowledgements

Financial support was provided by the National Science Foundation (CHE 1707660 to A. S.) and by Omicron Biochemicals, Inc., South Bend, IN. The Notre Dame Radiation Laboratory is supported by the Department of Energy Office of Science, Office of Basic Energy Sciences under Award Number DE-FC02-04ER15533. This is document number NDRL 5224.

Supporting Information

Chemical synthesis protocols for ^{13}C-labeled **2–4**; HRMS data for ^{13}C-labeled **2-4**; ^{13}C{^{1}H} NMR spectra of $\mathbf{3}^{1,2}$, $\mathbf{3}^{1,3}$, $\mathbf{3}^{1,6}$, $\mathbf{2}^{1',5}$ and $\mathbf{4}^{1',5}$; torsional constraints applied to $\mathbf{2}^{k}$ and $\mathbf{4}^{k}$ during DFT calculations**;** ^{1}H-^{1}H spin-couplings in **2–4**; fitting statistics from solid-state ^{13}C NMR determinations of J_{CC} values; contour plots of DFT-calculated $^{3}J_{C1,C6}$ values in $\mathbf{3}^{k}$; experimental J_{CC} in $\mathbf{3}^{1,2}$, $\mathbf{3}^{1,3}$, $\mathbf{3}^{1,6}$, and J_{CC} values calculated by DFT in different *in silico* models of **3**; plots of $^{3}J_{C1',C5}$ against ψ in $\mathbf{2}^{k}$ and $\mathbf{4}^{k}$; Cartesian coordinates for $\mathbf{2}^{k}$–$\mathbf{4}^{k}$; complete reference 40.

References

1. N. Müller and D. E. Pritchard, C^{13} Splittings in Proton Magnetic Resonance Spectra. I. Hydrocarbons, *J. Chem. Phys*. 1959, **31**, 768–771.
2. P. E. Hansen, Carbon-Hydrogen Spin-Spin Coupling Constants, *Prog. Nucl. Magn. Reson. Spectrosc*. 1981, **14**, 175–295.
3. R. H. Contreras and J. E. Peralta, Angular Dependence of Spin-Spin Coupling Constants, *Prog. Nucl. Magn. Reson. Spectrosc*. 2000, **37**, 321–425.
4. N. Marco, A. A. Souza, P. Nolis, C. Cobas, R. R. Gil and T. Parella, $^{1}J_{CH}$ NMR Profile: Identification of Key Structural Features and Functionalities by Visual Observation and Direct Measurement of One-Bond Proton-Carbon Coupling Constants, *J. Org. Chem.* 2017, **82**, 2040–2044.
5. G. E. Maciel, J. W. McIver, N. S. Ostlund and J. A. Pople, Approximate Self-Consistent Molecular Orbital Theory of Nuclear Spin Coupling. III. Geminal Proton-Proton Coupling Constants, *J. Am. Chem. Soc.* 1970, **92**, 4151–4157.
6. I. Ando and G. A. Webb, *Theory of NMR Parameters*. Academic Press, New York, 1983, 106–107.
7. M. Karplus, Contact Electron-Spin Coupling of Nuclear Magnetic Moments, *J. Chem. Phys*. 1959, **30**, 11–15.

8. R. U. Lemieux, R. K. Kullnig, H. J. Bernstein and W. G. Schneider, Configurational Effects on the Proton Magnetic Resonance Spectra of Six-Membered Ring Compounds, *J. Am. Chem. Soc.* 1958, **80**, 6098–6105.

9. M. J. Hadad, W. Zhang, T. Turney, L. Sernau, X. Wang, R. J. Woods, A. Incandela, I. Surjancev, A. Wang, M.-K. Yoon, A. Coscia, C. Euell, R. Meredith, I. Carmichael and A. S. Serianni, NMR Spin-Couplings in Saccharides: Relationships Between Structure, Conformation and the Magnitudes of J_{HH}, J_{CH} and J_{CC} Values. *New Developments in NMR 10: NMR in Glycoscience and Glycotechnology*, Peters, T., Kato, K., eds., Royal Society of Chemistry, 2017, 20–100.

10. T. Klepach, H. Zhao, X. Hu, W. Zhang, R. Stenutz, M. J. Hadad, I. Carmichael and A. S. Serianni, Informing Saccharide Structural NMR Studies with Density Functional Theory Calculations. In: *Glycoinformatics: Methods in Molecular Biology*. Lütteke, T., Frank, M. eds., Springer, New York, 2015, 289–331.

11. I. Carmichael, D. M. Chipman, C. A. Podlasek and A. S. Serianni, Torsional Effects on the One-Bond ^{13}C-^{13}C Spin Coupling Constant in Ethylene Glycol: Insights Into the Behavior of $^{1}J_{CC}$ in Carbohydrates, *J. Am. Chem. Soc.* 1993, **115**, 10863–10870.

12. J. Wu, P. B. Bondo, T. Vuorinen and A. S. Serianni, ^{13}C-^{13}C Spin Coupling Constants in Aldoses Enriched with ^{13}C at the Terminal Hydroxymethyl Carbon: Effect of Coupling Pathway Structure on J_{CC} in Carbohydrates, *J. Am. Chem. Soc.* 1992, **114**, 3499–3505.

13. B. Bose-Basu, T. Klepach, G. Bondo, P. B. Bondo, W. Zhang, I. Carmichael and A. S. Serianni, ^{13}C-^{13}C NMR Spin-Spin Coupling Constants in Saccharides: Structural Correlations Involving All Carbons In Aldopyranosyl Rings, *J. Org. Chem.* 2007, **72**, 7511–7522.

14. F. Cloran, I. Carmichael and A. S. Serianni, Density Functional Calculations on Disaccharide Mimics: Studies of Molecular Geometries and Trans-*O*-Glycosidic $^{3}J_{COCH}$ and $^{3}J_{COCC}$ Spin-Couplings, *J. Am. Chem. Soc.* 1999, *121*, 9843–9851.

15. M. J. Duer, ed. *Solid State NMR Spectroscopy: Principles and Applications*, John Wiley & Sons, 2008 DOI: 10.1002/9780470999394.

16. M. Mehring, *Principles of High Resolution NMR in Solids*, Springer-Verlag, Berlin, Heidelberg, New York, 1983, DOI: 10.1007/978-3-642-68756-3.

17. I. Wawer and S. Witkowski, Analysis of Solid State ^{13}C NMR Spectra of Biologically Active Compounds, *Curr. Org. Chem.* 2001, **5**, 987–999.

18. S. P. Brown, M. Pérez-Torralba, D. Sanz, R. M. Claramunt and L. Emsley, The Direct Detection of a Hydrogen Bond in Solid State by NMR Through the Observation of a Hydrogen-Bond Mediated ^{15}N–^{15}N *J* Coupling, *J. Am. Chem. Soc.* 2002, **124**, 1152-1153.

19. G. De Paepe, A. Lesage and L. Emsley, The Performance of Phase Modulated Heteronuclear Dipolar Decoupling Schemes in Fast Magic-Angle-Spinning Nuclear Magnetic Resonance Experiments, *J. Chem. Phys.* 2003, **119**, 4833–4841.

20. T. N. Pham, J. M. Griffin, S. Masiero, S. Lena, G. Gottarelli, P. Hodgkinson, C. Filip and S. P. Brown, Quantifying Hydrogen-Bonding Strength: The Measurement of $^{2h}J_{NN}$ Couplings in Self-Assembled Guanosines by Solid-State ^{15}N Spin-Echo MAS NMR, *Phys. Chem. Chem. Phys.* 2007, **9,** 3416–3423.

21. R. Challoner, T. Nakai and C. A. McDowell, *J* Coupling in Chemically Equivalent Spin Pairs as Studied by Solid-State Nuclear Magnetic Resonance, *J. Chem. Phys.* 1991, **94**, 7038–7045.

22. G. Wu and R. E. Wasylishen, Homonuclear Phosphorus-31 *J*-Resolved 2D Spectra of Rhodium (I) Phosphine Complexes in the Solid State, *Inorg. Chem.* 1992, **31**, 145–148.

23. T. N. Pham, S. Masiero, G. Gottarelli and S. P. Brown, Identification by ^{15}N Refocused INADEQUATE MAS NMR of Intermolecular Hydrogen Bonding That Directs the Self-Assembly of Modified DNA Bases, *J. Am. Chem. Soc.* 2005, **127**, 16018–16019.

24. H. M. Foucault, D. L. Bryce and D. E. Fogg, A Chelate-Stabilized Ruthenium Complex: Resolving Ambiguities in Nuclearity and Coordination Geometry Through ^{1}H PGSE and ^{31}P Solid-State NMR Studies, *Inorg. Chem.* 2006, **45**, 10293–10299.

25. S. P. Brown, M. Perez-Torralba, D. Sanz, R. M. Claramunt and L. Emsley, Determining Hydrogen-Bond Strengths in the Solid State by NMR: The Quantitative Measurement of Homonuclear *J* Couplings, *Chem. Commun.* 2002, 1852–1853.

26. S. Cadars, A. Lesage, N. Hedin, B. F. Chmelka and L. Emsley, Selective NMR Measurements of Homonuclear Scalar Couplings in Isotopically Enriched Solids, *J. Phys. Chem. B* 2006, **110**, 16982–16991.

27. W. C. Lai, N. McLean, A. Gansmüller, M. A. Verhoeven, G. C. Antonioli, M. Carravetta, L. Duma, P. H. Bovee-Geurts, O. G. Johannessen, H. J. de Groot, J. Lugtenburg, L. Emsley, S. P. Brown, R. C. D. Brown, W. J. DeGrip and M. H. Levitt, Accurate Measurements of ^{13}C–^{13}C *J*-Couplings in the Rhodopsin Chromophore by Double-Quantum Solid-State NMR Spectroscopy, *J. Am. Chem. Soc.* 2006, **128**, 3878–3879.

28. S. P. Brown and L. Emsley, The 2D MAS NMR Spin-Echo Experiment: The Determination of ^{13}C–^{13}C *J* Couplings in a Solid-State Cellulose Sample, *J. Magn. Reson.* 2004, **171**, 43-47.

29. J. Becker-Baldus, T. F. Kemp, J. Past, A. Reinhold, A. Samoson and S. P. Brown, Longer-Range Distances by Spinning-Angle-Encoding Solid-State NMR Spectroscopy, *Phys. Chem. Chem. Phys.* 2011, **13**, 4514–4518.

30. P. Thureau, G. Mollica, F. Ziarelli and S. Viel, Selective Measurements of Long-Range Homonuclear *J*-Couplings in Solid-State NMR, *J. Magn. Reson.* 2013, **231**, 90–94.

31. G. A. Jeffrey and S. Takagi, The Crystal and Molecular Structure of Methyl β-D-Glucopyranoside Hemihydrate, *Acta Cryst.* 1977, **B33**, 738–742.

32. Q. Pan, B. C. Noll and A. S. Serianni, Methyl 4-*O*-β-D-Galactopyranosyl α-D-glucopyranoside (Methyl α-Lactoside), *Acta Cryst*. 2005, **C61**, o674–o677.

33. R. Stenutz, M. Shang and A. S. Serianni, Methyl β-Lactoside (Methyl 4-*O*-β-D-Galactopyranosyl-β-D-glucopyranoside) Methanol Solvate, *Acta Cryst*. 1999, **C55**, 1719–1721.

34. D. Cremer and J. A. Pople, General Definition of Ring Puckering Coordinates, *J. Am. Chem. Soc*. 1975, **97**, 1354–1358.

35. B. Bose, S. Zhao, P. Bondo, G. Bondo, F. Cloran, I. Carmichael, R. Stenutz, B. Hertz and A. S. Serianni, Three-Bond C–O–C–C Spin-Coupling Constants in Carbohydrates: Development of a Karplus Relationship, *J. Am. Chem. Soc.* 1998, **120**, 11158–11173.

36. A. S. Serianni, H. A. Nunez and R. Barker, Carbon-13-Enriched Carbohydrates. Preparation of Aldononitriles and Their Reduction with a Palladium Catalyst, *Carbohydr. Res*. 1979, **72**, 71–78.

37. W. Zhang, S. Zhao and A. S. Serianni, Labeling Monosaccharides with Stable Isotopes, *Methods Enzymol.* 2015, **565**, 423–458.

38. M. L. Hayes, N. J. Pennings, A. S. Serianni and R. Barker, Epimerization of Aldoses by Molybdate Involving a Novel Rearrangement of the Carbon Skeleton, *J. Am. Chem. Soc.* 1982, **104**, 6764–6769.

39. M. J. King-Morris, P. B. Bondo, R. A. Mrowca and A. S. Serianni, Stable Isotopically Substituted Carbohydrates: An Improved Synthesis of (6-^{13}C)Aldohexoses, *Carbohydr. Res.* 1988, **175**, 49–58.

40. M. J. Frisch, *et al*., *Gaussian*09, *Revision D*, 2009, Gaussian Inc.: Wallingford, CT, 2009.

41. A. D. Becke, Density-Functional Thermochemistry. III. The Role of Exact Exchange, *J. Chem. Phys.* 1993, **98**, 5648–5652.

42. A. D. Becke, New Mixing of Hartree-Fock and Local Density-Functional Theories, *J. Chem. Phys*. 1993, **98**, 1372–1377.

43. W. J. Hehre, R. Ditchfield and J. A. Pople, Self-Consistent Molecular Orbital Methods. XII. Further Extensions of Gaussian-Type Basis Sets for Use in Molecular Orbital Studies of Organic Molecules, *J. Chem. Phys.* 1972, **56**, 2257–2261.

44. E. Cances, B. Mennucci and J. Tomasi, A New Integral Equation Formalism for the Polarizable Continuum Model: Theoretical Background and Applications To Isotropic and Anisotropic Dielectrics, *J. Chem. Phys.* 1997, **107**, 3032–3041.

45. R. Cammi, B. Mennucci and J. Tomasi, Fast Evaluation of Geometries and Properties of Excited Molecules in Solution: A Tamm-Dancoff Model with Application to 4-Dimethylaminobenzonitrile, *J. Phys. Chem.* 2000, **A104**, 5631–5637.

46. J.-P. Praly and R. Lemieux, Influence of Solvent on the Magnitude of the Anomeric Effect, *Can. J. Chem.* 1987, **65**, 213–223.

47. H. Thøgersen, R. U. Lemieux, K. Bock and B. Meyer, Further Justification for the *Exo* Anomeric Effect. Conformational Analysis Based on Nuclear Magnetic Resonance Spectroscopy of Oligosaccharides, *Can. J. Chem*. 1982, **60**, 44–57.

48. A. J. Kirby, *The Anomeric Effect and Related Stereoelectronic Effects at Oxygen*, Springer Verlag, Berlin, 1983 DOI: 10.1007/978-3-642-68676-4.

49. I. V. Alabugin, *Stereoelectronic Effects. A Bridge Between Structure and Reactivity*, John Wiley & Sons, West Sussex, UK, 2016, DOI: 10.1002/9781118906378.

50. V. Sychrovsky, J. Grafenstein and D. Cremer, Nuclear Magnetic Resonance Spin–Spin Coupling Constants from Coupled Perturbed Density Functional Theory, *J. Phys. Chem*. 2000, **113**, 3530–3547.

51. T. Helgaker, M. Watson and N. C. Handy, Analytical Calculation of Nuclear Magnetic Resonance Indirect Spin–Spin Coupling Constants at the Generalized Gradient Approximation and Hybrid Levels of Density-Functional Theory, *J. Chem. Phys.* 2000, **113**, 9402–9409.

52. V. Barone, J. E. Peralta, R. H. Contreras and J. P. Snyder, DFT Calculation of NMR J_{FF} Spin–Spin Coupling Constants in Fluorinated Pyridines, *J. Phys. Chem.* 2002*,* **A106**, 5607–5612.

53. R. Stenutz, I. Carmichael, G. Widmalm and A. S. Serianni, Hydroxymethyl Group Conformation in Saccharides: Structural Dependencies of $^{2}J_{HH}$, $^{3}J_{HH}$ and $^{1}J_{CH}$ Spin-Spin Coupling Constants, *J. Org. Chem*. 2002, **67**, 949–958.

54. W. Zhang, T. Turney, R. Meredith, Q. Pan, L. Sernau, X. Wang, X. Hu, R. J. Woods, I. Carmichael and A. S. Serianni, Conformational Populations of β–(1→4) *O*-Glycosidic Linkages Using Redundant NMR *J*-Couplings and Circular Statistics, *J. Phys. Chem. B* 2017, **121**, 3042–3058.

55. W. Zhang, R. Meredith, Q. Pan, X. Wang, R. J. Woods, I. Carmichael and A. S. Serianni, Use of Circular Statistics To Model αMan-(1→2)-αMan and αMan-(1→3)-α/βMan *O*-Glycosidic Linkage Conformation in ^{13}C-Labeled Disaccharides and High-Mannose Oligosaccharides, *Biochemistry* 2019, **58**, 546–560.

56. T. Church, I. Carmichael and A. S. Serianni, Two-Bond ^{13}C-^{13}C Spin-Coupling Constants in Carbohydrates: Effect of Structure on Coupling Magnitude and Sign, *Carbohydr. Res*. 1996, **280**, 177–186.

57. A. S. Serianni, P. B. Bondo and J. Zajicek, Verification of the Projection Resultant Method for Two-Bond ^{13}C-^{13}C Coupling Sign Determinations in Carbohydrates, *J. Magn. Reson.* 1996, **B112**, 69–74.

58. W. Zhang, A. G. Oliver, H. M. Vu, J. G. Duman and A. S. Serianni, Methyl 4-*O*-β-D-Mannopyranosyl β-D-xylopyranoside, *Acta Cryst*. 2012, **C68**, o502–506.

59. W. Zhang, A. G. Oliver and A. S. Serianni, Disorder and Conformational Analysis of Methyl β-D-galactopyranosyl-(1→4)-β-D-xylopyranoside, *Acta Cryst*. 2012, **C68**, o7–o11.

60. S. A. Joyce, J. R. Yates, C. J. Pickard and F. Mauri, A First Principles Theory of Nuclear Magnetic Resonance *J*-Coupling in Solid-State Systems, *J. Chem. Phys.* 2007, **127**, 204107.

61. S. A. Joyce, J. R. Yates, C. J. Pickard and S. P. Brown, Density Functional Theory Calculations of Hydrogen-Bond-Mediated NMR *J* Coupling in the Solid State, *J. Am. Chem. Soc.* 2008, **130**, 12663–12670.

62. C. E. Hughes, G. N. M. Reddy, S. Masiero, S. P. Brown, P. A. Williams and K. D. M. Harris, Determination of a Complex Crystal Structure in the Absence of Single Crystals: Analysis of Powder X-ray Diffraction Data, Guided by Solid-State NMR and Periodic DFT Calculations, Reveals a New 2′-Deoxyguanosine Structural Motif, *Chem. Sci.* 2017, **8**, 3971–3979.

63. H. Zhao, Q. Pan, W. Zhang, I. Carmichael and A. S. Serianni, DFT and NMR Studies of $^{2}J_{COH}$, $^{3}J_{HCOH}$ and $^{3}J_{CCOH}$ Spin-Couplings in Saccharides: C–O Torsional Bias and H-Bonding in Aqueous Solution, *J. Org. Chem*. 2007, **72**, 7071–7082.

64. C. Thibaudeau, R. Stenutz, B. Hertz, T. Klepach, S. Zhao, Q. Wu, I. Carmichael and A. S. Serianni, Correlated C–C and C–O Bond Conformations in Saccharide Hydroxymethyl Groups: Parameterization and Application of Redundant ^{1}H-^{1}H, ^{13}C-^{1}H and ^{13}C-^{13}C NMR *J*-Couplings, *J. Am. Chem. Soc*. 2004, **126**, 15668–15685.

65. P. Guerry, M. E. Smith and S. P. Brown, ^{31}P MAS Refocused INADEQUATE Spin-Echo (REINE) NMR Spectroscopy: Revealing *J* Coupling and Chemical Shift Two-Dimensional Correlations in Disordered Solids, *J. Am. Chem. Soc.* 2009, **131**, 11861–11874.

66. P. Guerry, S. P. Brown and M. E. Smith, Improving the Sensitivity of *J* Coupling Measurements in Solids with Application to Disordered Materials, *AIP Advances* 2016, **6**, 055008.

67. D. Sakellariou, S. P. Brown, A. Lesage, S. Hediger, M. Bardet, C. A. Meriles, A. Pines and L. Emsley, High-Resolution NMR Correlation Spectra of Disordered Solids, *J. Am. Chem. Soc.* 2003, **125**, 4376–4380.

TOC Graphic

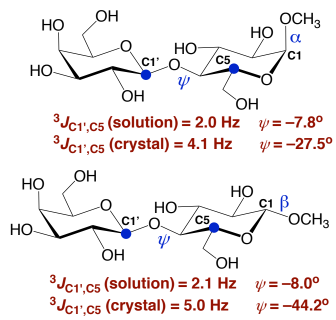

● = ^{13}C

Solid-state ^{13}C NMR reveals quantitative differences in *O*-glycosidic linkage conformation in solution and in crystalline disaccharides. Experimental J_{CC} values in crystalline samples provide a means of validating J_{CC} values calculated from density functional theory.

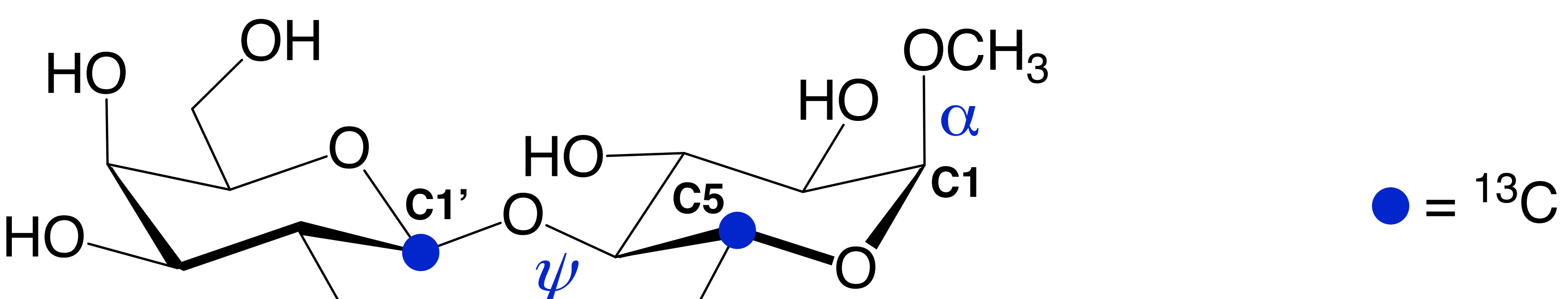
OH
HO
HO
O
C1'
O
ψ
HO
C5
HO
OCH3
α
C1
O
= 13C

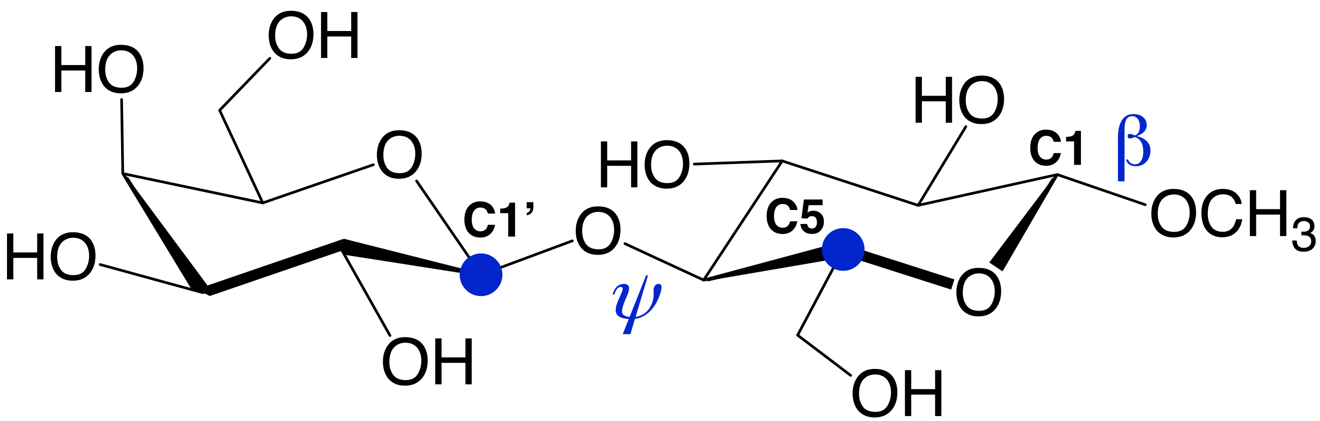

$^3J_{C1',C5}$ **(solution) = 2.1 Hz** $\psi = -8.0^o$

$^3J_{C1',C5}$ **(crystal) = 5.0 Hz** $\psi = -44.2^o$

conformation in so
in crystalline disac
Experimental J_{CC}
crystalline sample
means of validatin
values calculated
density functional